DOI: 10.1002/chem.200600781

Structural, Solid-State NMR and Theoretical Studies of the Inverse-Coordination of Lithium Chloride Using Group 13 Phosphide Hosts

Melinda J. Duer,[a] Felipe García,[a] Jonathan M. Goodman,[a] Jörg P. Hehn,[a] Richard A. Kowenicki,[a] Vesal Naseri,[a] Mary McPartlin,[b] Matthew L. Stead,[a] Robin Stein,[a] and Dominic S. Wright*[a]

Abstract: The reaction of $MeAlCl_2$ with 'PhPLi$_2$' in THF gives [{MeAl(PPh)$_3$Li$_4$·3THF}$_4$(μ_4-Cl)]$^-$Li$^+$ (**1**). The Ga^{III} and In^{III} analogues, [{MeE(PPh)$_3$Li$_4$·3THF}$_4$(μ_4-Cl)]$^-$Li$^+$·(THF)$_3$ (E = Ga (**2**), In (**3**)), are obtained by the in situ reactions of $MeECl_2$ with $PhPLi_2$ in THF. For all of the complexes, the cage anions have an unusual cubic arrangement that is similar to a zeolite, and contain large voids (ca. 17 Å). The location of the Li$^+$ counterions in **1**–**3** and their coordination environment appears to subtly reflect variations in packing and lattice energy. Whereas in **1** highly mobile, loosely coordinated Li$^+$ counterions are present, **2** and **3** contain less mobile THF-solvated counterions within the cavities. X-ray crystallographic and solid-state NMR studies are reported on **1**–**3**, together with model DFT calculations on the selectivity of halide coordination.

Keywords: cage compounds · Group 13 elements · main group elements · structure elucidation

Introduction

There is considerable interest in the effects of modifying the structures of ionic compounds into molecular arrangements to give materials with unusual properties such as low melting points and solubility in organic solvents.[1] Such studies have been motivated particularly by the search for new, lightweight battery materials and for low-energy routes to metals.[2] The most obvious way by which fragmentation of an ionic lattice can be achieved is by replacing some or all of the cation–anion bonding with Lewis base coordination (Figure 1).[1] In notable cases, the molecular species produced bear a close resemblance to the parent lattice. For example, in situ generation of LiCl in the presence of the Lewis base donor HMPA (HMPA = $(Me_2N)_3P{=}O$)] gives [LiCl·HMPA]$_4$, whose cubane structure represents an extruded fragment of the parent lattice of LiCl.[3] A further strategy is the confinement of a salt lattice within another framework. Recent interest in this area has focused on the growth of salt lattices within carbon nanotubes (Figure 1).[4] Remarkably, completely novel lattice arrangements can be formed which are different to those of the bulk starting materials. A third way by which alkali metal salt lattices can be

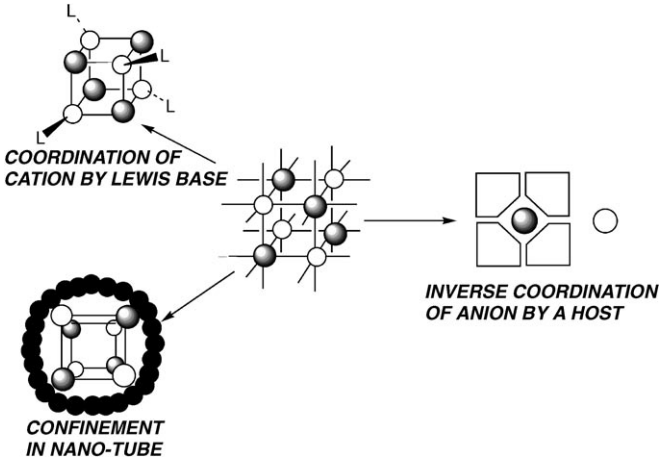

Figure 1. Modification of ionic lattices, illustrated for the fragmentation of the NaCl-type lattice.

[a] Dr. M. J. Duer, Dr. F. García, Dr. J. M. Goodman, J. P. Hehn, R. A. Kowenicki, V. Naseri, M. L. Stead, R. Stein, Dr. D. S. Wright
Chemistry Department, Cambridge University
Lensfield Road, Cambridge CB2 1EW (UK)
Fax: (+44) 1223-336-362
E-mail: dsw1000@cus.cam.ac.uk

[b] Prof. M. McPartlin
Department of Health and Biological Sciences
London Metropolitan University, London N7 8DB (UK)

Supporting information for this article is available on the WWW under http://www.chemeurj.org/ or from the author.

modified is by coordination of the anion (Figure 1). This approach is the opposite to the conventional coordination of the cation using a Lewis base and thus (based on Mulvey's terminology)[5] can be termed *inverse coordination*. Although there are many examples of anion receptors based on organic frameworks, in such organic systems anion–receptor interactions are relatively weak compared to the lattice energies of simple metal salts.[6] The obvious candidates for *strong* anion receptors are inorganic metal hosts. Recent studies by Mulvey et al.[5] and Hawthorne et al.[7] have illustrated the power of inverse coordination of this type using macrocyclic hosts. Hawthorne has developed a series of metallacarborand hosts composed of $C_{10}B_2$ icosahedra which are linked together into macrocycles by bridging Hg^{II} atoms, the latter functioning as acceptor sites to a range of anions. Mulvey and co-workers have explored a range of Group 1, 2 and 12 macrocyclic hosts (so-called "inverse crowns") that are capable of stabilising hitherto unknown anions.[5] The work of Zheng and co-workers is also worthy of mention in this context, involving templating and modification of ionic systems using various anions.[8]

Results and Discussion

Synthesis and characterisation of 1–3: Our interest in this area has arisen from a long-term interest in the structural and materials properties of p-block metal phosphides.[9] We recently became interested in the synthesis of Group 13 anions of the type $[RE(PR)_3]^{4-}$ (E = Al, Ga, In).[10] In a recent communication we reported that the crystalline product obtained in 43% (first batch) yield from the reaction of $'PhPLi_2'$ with $MeAlCl_2$ in THF is the ion-separated compound $Li^+[\{MeAl(PPh)_3Li_4{\cdot}3THF\}_4(\mu_4\text{-}Cl)]^-$ (**1**) (Scheme 1).[11] In view of the lack of availability of the analogous starting materials $MeECl_2$ and the difficulty in preparing these highly air-sensitive materials for the heavier Group 13 elements, we adopted an in situ approach to the Ga^{III} and In^{III} analogues. The stepwise reactions of ECl_3 (E = Ga, In) with MeLi followed by reaction with $'PhPLi_2'$[12] give crystals of the desired Ga and In complexes, **2** and **3**, respectively, which are tentatively formulated as $(Li^+)^1/_3[(THF)_3Li^+]^2/_3[\{MeGa(PPh)_3Li_4{\cdot}3THF\}_4(\mu_4\text{-}Cl){\cdot}12THF]^-{\cdot}THF$ and $[(THF)_3Li]^+[\{MeIn(PPh)_3Li_4{\cdot}3THF\}_4(\mu_4\text{-}Cl){\cdot}12THF]^-$, respectively (Scheme 2). The low yields of **2** and **3** obtained (16 and 5.5%, respectively) are either the result of the inefficiency of the in situ reactions involved in their formation or of the necessity to extract the crude products into Et_2O during workup (in which neither complex is very soluble). The presence of labile THF solvent molecules in both complexes and their extreme air sensitivity resulted in some variation in the analytical results and satisfactory results (to within 0.5%) could not be obtained despite repeated attempts. The room-temperature ^{31}P NMR spectra in THF of **2** and **3** both show singlets at $\delta = -150.5$ and -166.1 ppm, respectively. These chemical shifts can be compared to the value of $\delta = -161.8$ ppm for the Al analogue **1** (also in THF, relative to 85% H_3PO_4/D_2O).[11] The lack of any obvious correlation between the chemical shift and position in Group 13 is perhaps unsurprising bearing in mind the complicated factors governing ^{31}P NMR chemical shifts.[13] However, it is nonetheless tempting to ascribe the disparate value for **2** to the onset of d-block contraction and its effect on metal charge density and electronegativity. The room-temperature ^7Li NMR spectra of **2** shows three singlets at $\delta = 2.16$, 1.75 and -0.55 ppm, whereas the spectrum of **3** exhibits two major resonances at $\delta = 1.44$ and -1.01 ppm and a shoulder at about $\delta = -0.6$ ppm. The appearance of the ^7Li NMR spectra of **2** and **3** do not change appreciably with concentration or temperature. However, it is difficult to assign these resonances unequivocally to each of the three ^7Li environments present in **2** and **3**.

Crystallographic studies: Low-temperature (180(2) K) X-ray crystallographic studies were undertaken on **1**, **2** and **3**. Although we have communicated the structure of **1** previously,[10] re-examination of the original data shows that the cage anion of this complex is in fact slightly disordered in a similar way to that found for the new complexes **2** and **3**. Table 1 gives the crystal data for **1**, **2** and **3**, which includes the new refinement of **1**. Key bond lengths and angles for **1** (from the new refinement), **2** and **3** are collected in Table 2 for comparison.

The solid-state structures of complexes **1–3** are very similar, all containing $[\{MeM(PPh)_3Li_4\}_4(\mu_4\text{-}Cl){\cdot}12THF]^-$ (M = Al, Ga or In, respectively) anions. The heterometallic cage anions of these complexes have $[E_4P_{12}Li_{16}(\mu_4\text{-}Cl)]$ cores in which an interstitial Cl^- ion is effec-

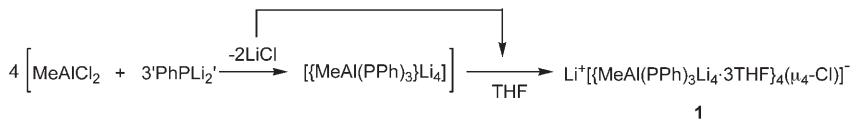

Scheme 1.

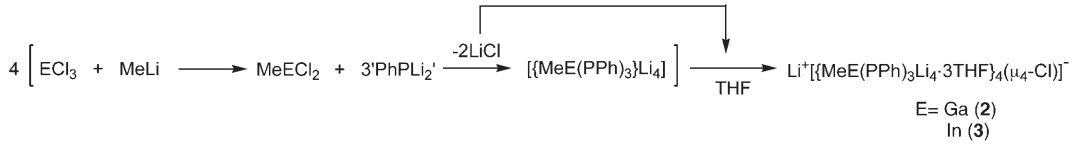

Scheme 2.

Table 1. Crystal data and structure refinements for **1**, **2** and **3**.[a]

	1	**2**	**3**
empirical formula	$C_{124}H_{168}Al_4ClLi_{17}O_{12}P_{12}$	$C_{136}H_{192}ClGa_4Li_{17}O_{15}P_{12}$	$C_{136}H_{192}ClIn_4Li_{17}O_{15}P_{12}$
fw	2483.57	2870.85	3051.25
crystal system	cubic	cubic	cubic
space group	$F\bar{4}3c$	$F\bar{4}3c$	$F\bar{4}3c$
a [Å]	35.037(4)	34.944(4)	35.252(4)
Z	8	8	8
V [Å^3]	43011(9)	42671(8)	43807(9)
ρ_{calcd} [Mg m^{-3}]	0.767	0.894	0.925
$\mu(Mo_{K\alpha})$ [mm^{-1}]	0.158	0.641	0.554
$F(000)$	10464	12000	12576
reflns. collected	10490	15653	8340
crystal size [mm]	0.30×0.23×0.21	0.31×0.30×0.23	0.14×0.12×0.07
θ range [°]	4.19–21.00	4.21–24.97	3.66–21.21
independent reflns.	1683	2991	1919
(R_{int})	(0.162)	(0.039)	(0.151)
absorption correction	semi-empirical from equivalents	semi-empirical from equivalents	semi-empirical from equivalents
max., min. transmission	0.969, 0.941	0.862, 0.748	0.964, 0.911
data/restraints/parameters	1683/0/116	2991/21/161	1919/37/133
goodness-of-fit on F^2	0.984	1.13	0.961
R indices [$I>2\sigma(I)$]			
$R1$	0.074	0.061	0.066
$WR2$	0.168	0.160	0.160
R indices (all data)			
$R1$	0.135	0.080	0.130
$WR2$	0.197	0.186	0.187
absolute structure parameter	0.20(11)	0.47(3) [twin]	0.20(14)
largest peak and hole [e Å^{-3}]	0.237, −0.218	0.061, −0.529	0.412, −0.329

[a] Data in common; $T=180(2)$ K, $\lambda=0.71073$ Å.

Table 2. Selected bond lengths [Å] and angles [°] for **1**, **2** and **3**.

	1	**2**	**3**
E(1)–C(10)	2.01(2)	2.013(8)	2.20(2)
E(1)–P(1)	2.461(3)	2.432(1)	2.601(4)
P–Li (range)	2.461(3)–2.71(2)	2.558(4)–2.641(10)	2.56(1)–2.66(3)
Li(2)–Cl(1)	2.45(2)	2.37(1)	2.46(3)
P-E(1)-P	103.0(1)	102.82(4)	100.81(9)
C(10)-E(1)-P(1)	115.33(9)	115.50(3)	117.15(7)
Li-Cl(1)-Li	109.5	109.5	109.5

tively coordinated by four $[MeE(PPh)_3Li_4]$ units (Figure 2a). Although templating of inorganic cages by halide ions has been seen before,[7] to our knowledge the coordination of the halide ion *only* is unique for a simple salt. Thus, the structures of **1**–**3** provide a dramatic illustration of the concept of inverse coordination.

The tetrahedral $[MeE(PPh)_3]^{4-}$ ions of **1**–**3** are arranged in a supramolecular tetrahedron (filled bonds, Figure 2b), which defines the polyhedral arrangement of Li^+ ions of the anions. The twelve phosphorus atoms of the cages are all six coordinate, each being bonded to four Li^+ ions within the core (2.47(2)–2.71(2) (**1**), 2.557(4)–2.641(10) (**2**) and 2.56(1)–2.66(3) Å (**3**)). The twelve symmetry-related ions Li(1) to Li(1K) (dashed bonds, Figure 2b) form an outer shell of ions that are each bonded to three phosphorus centres and to the oxygen atom of a THF ligand. The inner shell of Li ions Li(2) to Li(2C) (grey bonds, Figure 2b) have a similar tetrahedral coordination environment, only now their four-coordinate geometry is completed by bonding to the central Cl^- anion (Li(2)–Cl(1) 2.46(2) (**1**), 2.37(1) (**2**) and 2.46(3) Å (**3**)) rather than to an O atom of a THF ligand.

The geometric parameters found in the anions of **1** and **2** are very similar, reflecting the very similar sizes of Al^{III} and Ga^{III} that result from d-block contraction. Although there is a small reduction in the E–P bond lengths (2.461(3) in **1**, 2.432(1) Å in **2**), the bridgehead P-E-P angles within the $[MeE(PPh)_3]^{4-}$ ions do not differ significantly (103.01(11) in **1**, 102.82(4)° in **2**). The net result is extremely similar bites for these two tripodal $[MeE(PPh)_3]^{4-}$ ions of 3.852(3) and 3.802(2) Å respectively, measured as the P···P separation within the anions. Thus, it is not surprising that the radii of the $[\{MeE(PPh)_3Li\}_4(\mu\text{-}Cl)]^-$ ions of **1** and **2** are almost identical (E···Cl 4.246(4) in **1**, 4.256(1) Å in **2**). However, the far greater radius of In results in much longer E–P bond lengths in **3**, In(1)–P(1) 2.601(4) Å. Although this effect is to some extent off-set by a decrease in the P-E-P angle within the $[MeIn(PPh)_3]^{4-}$ ion (P-In-P 100.81(9)°), there is a significant increase (ca. 0.15–0.20 Å) in the bite of the anion (P···P 4.008(5) Å), allowing an expansion of the surface of the cluster. The net result is an increase in the spherical radius of the $[\{MeIn(PPh)_3Li\}_4(\mu\text{-}Cl)]^-$ ion (In(1)···Cl(1) 4.407(1) Å) compared to the Al and Ga counterparts (mean 4.25 Å). It can be noted that previously reported lithium complexes containing analogous nitrogen $[RAl(NAr)_3]^{4-}$ tetraanions contain cage anions of the type $[\{RAl(NAr)_3\}_2Li_6]^{2-}$, in which no templating by Cl^- ions occurs (even though Cl^- ions may be present during their formation).[9,13] This difference compared to the structures of **1**, **2** and **3** appears to be due to the smaller ligand bite of the $[RAl(NAr)_3]^{4-}$ tetraanions (2.91 Å, measured as the N···N separation),[9] making the formation of larger spherical anions such as those present in **1**–**3** unfavourable (cf. ligand bites of 3.802(2)–4.008(5) Å for the $[MeE(PPh)_3]^{4-}$ tetraanions).

Evidence from the X-ray studies of **1**, **2** and **3** shows that the only structural difference between these species is in the location and solvation of the Li^+ counterion. A single Li^+ countercation is present in the lattice of **1** for each of the eight cage anions per unit cell, but owing to the high cubic symmetry of the lattices (96 equivalent positions) there is inherent uncertainty as to its location. For **1** the possibility

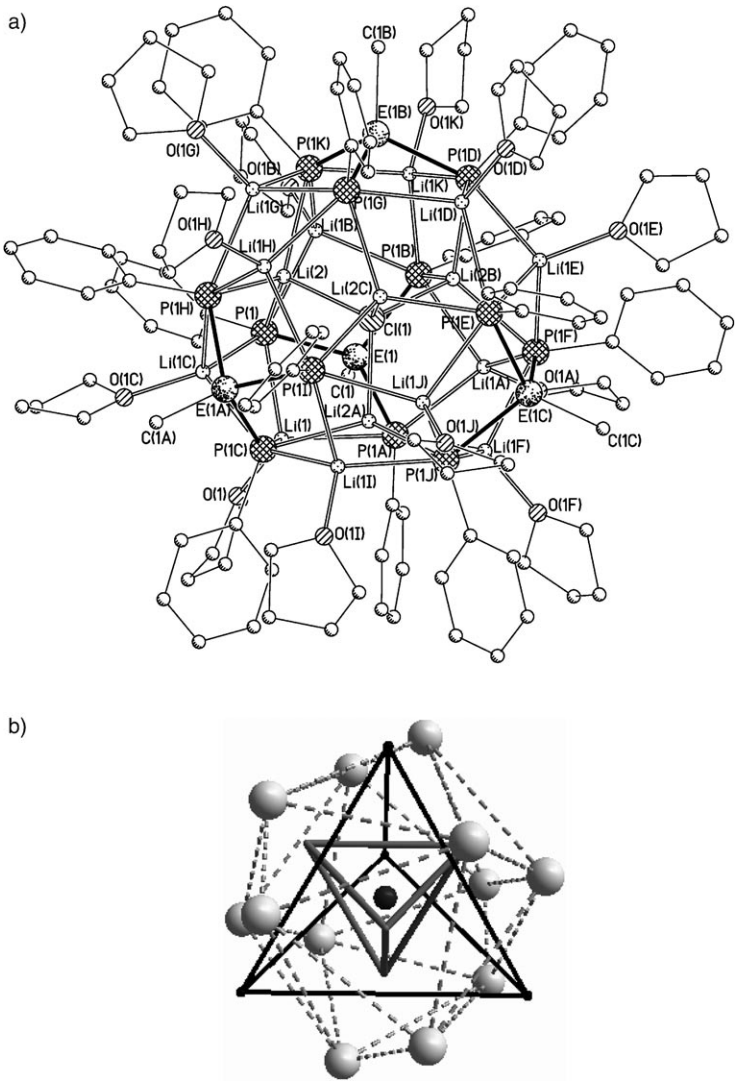

Figure 2. a) Structure of the heterometallic anions of **1**–**3** (E = Al (**1**), Ga (**2**), In (**3**)); symmetry transformations used to generate equivalent atoms: A: $x, -y+1, -z+1$; B: $-x+1, -y+1, z$; C: $-x+1, y, -z+1$; D: $-z+1, x, -y+1$; E: $y, -z+1, -x+1$; F: z, x, y; G: y, z, x; H: $-z, -x+1, -y+1$; I: $-z+1, -x+1, y$; J: $-y+1, -z+1, x$; K: $-y+1, z, -x+1$. b) Polyhedral Li (outer-shell; grey, dashed bonds), Al (black, filled bonds) and Li (inner-shell; grey, filled bonds).

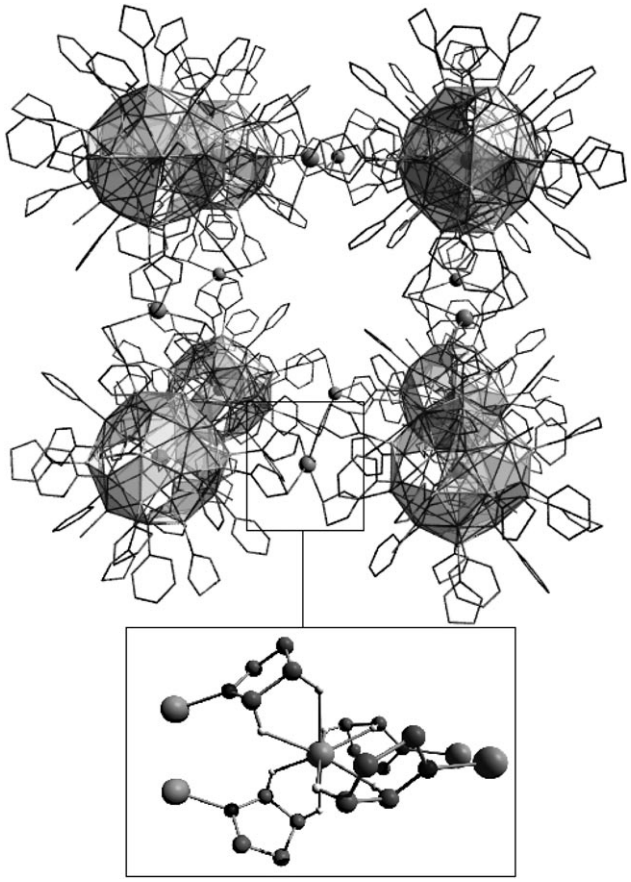

Figure 3. Formation of cube-shaped cavities within the structure of **1**, showing the partial-occupancy Li(3) sites between adjacent cluster anions (the insert shows the THF C–H···Li^+ interactions anchoring the Li^+ counterions in the lattice [C···Li 2.85, 3.17(2) Å)]).

that a highly disordered, solvated $[Li(THF)_n]^+$ ion (not detectable in the X-ray study) might be located in the cavity can be excluded on the basis of elemental analysis and ^1H NMR investigations of **1** before *and* after isolation of the complex under vacuum. The most likely location of Li^+ in **1** is midway between cluster anions (along the edges of the cubic unit cell or the central face-to-face diagonals, at $^1/_4$, 0, 0 (site symmetry -4)), with $^1/_3$ Li^+ occupancy in each of these twenty-four symmetry related sites (balancing the -8 charge of the eight anions present in the unit cell) (Figure 3). In **1** each Li^+ ion loosely binds two cluster anions together through agostic C–H···Li interactions with symmetry-related THF molecules (C(3),C(4)···Li(1) 2.85, 3.17(2), Å).[14] These interactions are typical of agostic C–H···Li bonding reported previously. The resulting lattice structure contains large voids (ca. 15 Å estimated from the centroid of the eight clusters forming the cube-shaped cavity to the closest contact) and has nearest-neighbour Li^+ and encapsulated Cl^- ions separated by 8.76 Å.

In the indium compound **3** there are three THF solvate molecules per cluster anion and from their grouping close together at bonding distance from a C_3 axis it was deduced that the Li^+ ion is present as a $[(THF)_3Li]^+$ ion of C_3 symmetry with 0.25 occupancy of the 32 equivalent sites (i.e. one per cluster anion). In the Ga compound **2** it appears that about $^2/_3$ of the Li^+ ions are present as $[(THF)_3Li]^+$ ions and the other $^1/_3$ are in edge sites midway between the cluster anions as deduced for the aluminium compound **1** (see Experimental Section). Although subsequent solid-state NMR spectroscopic studies are not entirely conclusive, they do provide overall support for the view that the Li^+ counterion is in a different position in **1** than in **2** and **3**.

An interesting feature of the lattice arrangement adopted by **1** in particular is its relationship to the well-known Linde Type A (LTA) structure of zeolites,[15] in which truncated octahedral units are bonded covalently into a 3D lattice at

their square faces (Figure 4a). Interestingly, the anions of **1**–**3** can be seen to be derived from a $P_{12}Li_{12}$ truncated cubo-octahedron (containing the symmetry-related Li(1) ions) in

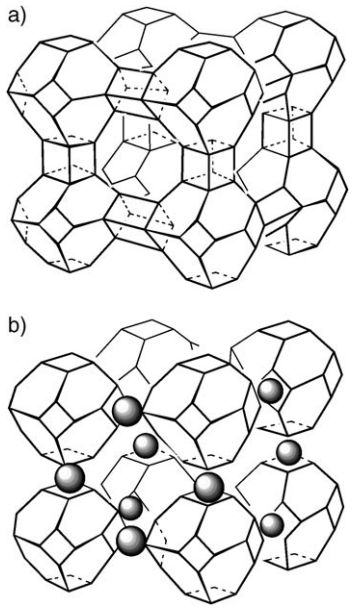

Figure 4. a) Zeolite Linde Type A structure, and b) schematic of the association of the anions in **1**.

which four tetrahedrally related P_3Li_3 faces are capped by the Group 13 metal centres (E), with the other four remaining P_3Li_3 faces bridged by the remaining four tetrahedrally related Li^+ ions Li(2). The lattice arrangement found for **1** is similar to the zeolite LTA,[15] only with square faces of the $P_{12}Li_{12}$ units being loosely linked by agostic interactions to Li(3) (Figure 4b). The presence of all the counterions in **3** as tris-solvated $[(THF)_3Li]^+$ complexes, in contrast to the edge location of the naked Li^+ ion in **1**, indicates that the maintenance of the same *pseudo*-primitive cubic arrangements for the large spherical anions in all three compounds **1**–**3** is dictated by minimisation of anion–anion repulsion and is independent of interactions with the counterion. Anion–anion repulsion would be significantly greater in any close-pack arrangements, which might have been expected for optimisation of anion–cation attraction.

Solid-state NMR studies: Solid-state NMR spectroscopy was used to help locate the lithium counterions in **1**, **2** and **3** and to confirm their crystal structures. ^7Li and ^{31}P NMR spectra were taken of all three compounds. ^{13}C NMR spectra were also taken of **2** and **3**, and a ^6Li NMR spectrum of **1** was also obtained. The presence of a mobile or naked lithium cation was confirmed in **1** using a saturation-recovery experiment to obtain ^7Li longitudinal relaxation time constants.[17–19] The ^7Li NMR spectrum (Table 3, Figure 5) contains two distinct regions, one with a relaxation time constant of about 6.2 s, and the other with a relaxation time constant of the order of 100 s. The second relaxation delay

Table 3. ^7Li chemical shift assignments and T_1 data for **1**, **2** and **3**.

Compound	Peak [ppm]	Assignment	T_1 [s]
Al	2.2	cage lithiums	6.2
	−1.2	mobile lithium	104
Ga	2.0	cage lithiums	16.5
	−0.1	"solvated" lithium	16.5
	−0.6	"solvated" lithium	16.5
In	2.5	cage lithiums	9
	0.5	"solvated" lithium (?)	9
	0.0	"solvated" lithium	9
	−0.6	"solvated" lithium	15.2

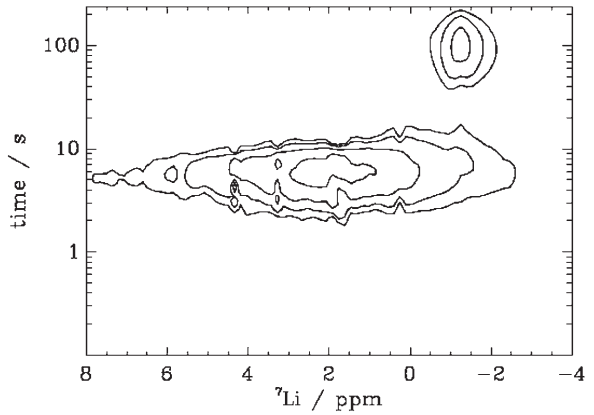

Figure 5. ^7Li relaxation-assisted separation (RAS) spectrum, demonstrating two ^7Li T_1 values for the Al complex **1**.

is surprisingly long, and is consistent with a lithium nucleus not interacting strongly with any other NMR-active nucleus. The broad region, with a shorter relaxation delay, can be assigned to the cage lithium atoms, on the basis of comparison with the ^6Li NMR spectrum and the $^7Li\{^1H\}$ cross-polarisation (CP) spectrum. The ^6Li NMR spectrum is shown in Figure 6 (see also Table 3). As expected, this spectrum shows narrower peaks than those in the ^7Li NMR spectrum as a result of the smaller quadrupolar moment of ^6Li. The spectrum can be broken down into two peaks corresponding to the lithium tetrahedral and dodecahedral cages. The mobile lithium does not appear in this spectrum, presumably because so many transients must be collected to obtain a

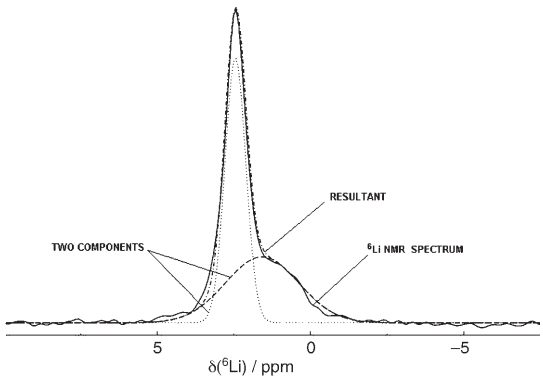

Figure 6. Solid-state ^6Li NMR spectrum and its breakdown into two peaks for the Al complex **1**.

signal that the slowly-relaxing component is saturated and does not give a signal. The ^{7}Li CP spectrum appears in Figure 7 (see also Table 3), along with a standard ^{1}H-decoupled ^{7}Li NMR spectrum, showing that the peak assigned to

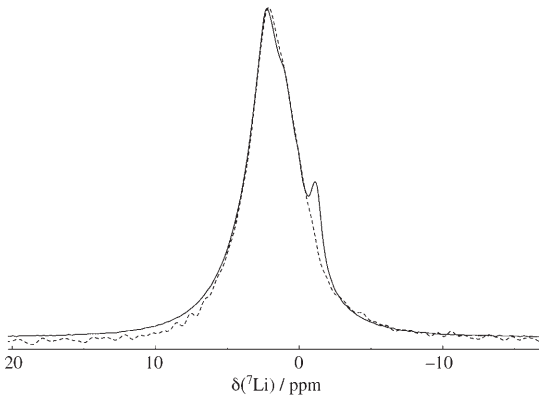

Figure 7. The ^{7}Li CP spectrum (solid lines) and ^{1}H-decoupled spectrum (dashed lines) of the Al complex **1**. The mobile lithium peak does not appear in the CP spectrum.

the mobile lithium is not present. CP spectra only show nuclei close in space to protons and not highly mobile.

In contrast to **1**, **3** appears to contain solvated lithium counteractions as revealed by its ^{7}Li saturation-recovery spectrum, with a long recovery delay of the order of 100 s (see Supporting Information). This shows sharp peaks in the spectrum of **3**, as appropriate for mobile lithium atoms tumbling isotropically in solution. THF signals also appear in the ^{13}C CP-TOSS spectrum [(CP with total suppression of spinning sidebands (TOSS)] of this analogue (see Supporting Information). Their isotropic chemical shifts are identical to those of bulk THF solution and their chemical shift anisotropy is small (no spinning sidebands appear when spinning at 6 kHz), so they appear liquid-like.

Neither the Ga (**2**) nor the In (**3**) analogues appears to contain any highly mobile/naked lithium ions. This is clear from their relaxation spectra (Figure 8 and Figure 9, respectively), which show that all lithium sites in each compound have a similar relaxation time, of the order of 10 s. Furthermore, no peak has the same chemical shift as the peak attributed to the mobile lithium in **1** (Figure 5, $\delta = -1.2$ ppm). The ^{7}Li NMR spectra indicate that **2** contains solvated lithium, like **3**. The ^{13}C NMR spectrum of **2** also contains the same THF peaks as **3** (see Supporting Information), supporting the existence of solvated lithium ions in the Ga analogue.

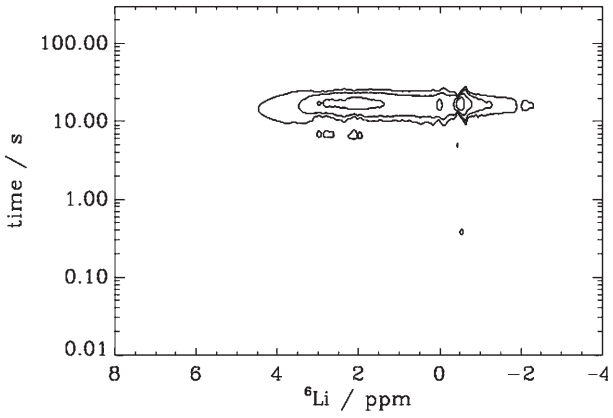

Figure 8. ^{7}Li relaxation-assisted separation (RAS) spectrum of the Ga complex **2**, showing a single T_1 relaxation time for the compound.

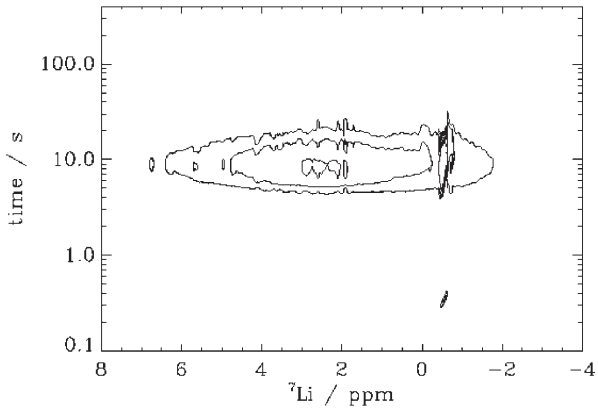

Figure 9. ^{7}Li relaxation-assisted separation (RAS) spectrum of the Ga complex **3**, showing a single T_1 relaxation time for the compound.

It is, however, possible that a small component of mobile/naked lithium, with a long relaxation delay, would not appear in either the ^{7}Li or the RAS spectrum. Simulations were used to determine whether a small component was likely to appear in the inverse Laplace transform of the relaxation spectrum.[20] The X-ray analysis of **2** suggests that approximately one-third of the Li^{+} counterion could be mobile, so a simulation was performed in which seven times as much signal had a relaxation time constant $T_1 = 10$ s as had $T_1 = 100$ s. Intensities for the curves were calculated for sixty values logarithmically distributed between 0.01 s and 300 s, as was used experimentally. It was found that if the Ga compound contains a long-relaxing component present in a ratio of 1:7 with a fast-relaxing component and with a signal-to-noise ratio of at least 200:1, the inverse Laplace transform should detect the long-relaxing component. The experimental spectrum shows no evidence of such a component, but this may be due to the spread of T_1 values likely to be present in the fast-relaxing component, or to the presence of both cage lithiums and solvated lithiums having T_1 of the order of 10 s, reducing the relative intensity of the long-relaxing component.

Solid-state ^{31}P NMR spectra were also acquired for **1**, **2** and **3**. Each compound appears to display a single phosphorus peak with a large manifold of spinning sidebands. Noticeably, the linewidths of these spectra are vastly different. The asymmetry in the spectrum of the In complex **3** may indicate the presence of a second, poorly resolved peak, suggesting that exchange is occurring between two sites in all three compounds, but at a much faster rate in the Ga analogue (**2**) than in the other two analogues. The ^{13}C NMR

spectrum of **2** also has slightly broader peaks than the spectrum of **3**. The ^{31}P isotropic chemical shifts of all three compounds are very similar to the values found in solution (for **1**: $\delta = -163.1$, **2**: -149.4, **3**: -165.6 ppm in the solid state; cf. **1**: -161.8, **2**: -150.5, **3**: -166.1 ppm in THF). Notably the chemical shift of the Ga complex (**2**) is again lower than the values found for the Al and In complexes, earlier ascribed to the onset of d-block contraction. From this similarity between the solid-state and solution studies it can be concluded that the structures of the anions of **1**, **2** and **3** are indeed retained in solution (as suggested by solution ^{7}Li and ^{31}P NMR studies described earlier). Since the spinning sideband intensity patterns in the solid-state ^{31}P NMR spectra of **1**, **2** and **3** are similar, the chemical shift anisotropies and asymmetries of the three compounds are similar, indicating that their chemical environments do not vary greatly in the solid state.

Theoretical calculations: DFT calculations at the B3LYP/LACVP** level[21,22] using Jaguar[23] were performed on the bare hosts $[\{HE(PH)_3Li_4{\cdot}3FH\}_4]$ and the cage anions $[\{HE(PH)_3Li_4{\cdot}3FH\}_4(\mu_4\text{-}X)]^-$ (E = B, Al, Ga, In; X = Cl, Br, I). For computational simplicity, the metal-bonded Me groups and Ph groups are replaced by H atoms and the THF solvation was replaced by HF. The species were constrained to *T*-symmetry, with the axes of the HF solvent molecules being constrained to point outwards from the centre of the cages. The calculations started from the coordinates of the core of the aluminium cage containing chloride (**1**), which did not undergo major changes on optimisation. The other structures came from re-minimising this structure after changing the elements (E and X) as required (see Supporting Information). Apart from providing an important lead to future studies, the primary questions we wished to address were 1) how does the enthalpy of coordination of X^- ions vary as Group 13 is descended?, and 2) what potential is there for the coordination and/or selection of other halide anions within this type of cage?

Selected bond lengths and angles for the models examined are presented in Table 4. Bearing in mind the simplifications of the computational models, the optimised structures of the chlorides of Al, Ga and In models (third row, Table 4) are close to those found experimentally (providing some validation of the models used). Overall, there are only small difference in the geometries predicted on changing the Group 13 element from In to Ga to Al for a particular halide ion incorporated, consistent with the structural trend observed experimentally for complexes **1**–**3**. The change to B leads to a slightly larger change in the cage geometry, as the B atom is rather closer to the centre of the cage than the larger Group 13 elements. Even in this case, however, the other elements within the cage are hardly perturbed by coordination of halide ions. For a particular Group 13 element (E), the main changes in the structures on changing the central halide ion are on the four, "inner-shell" Li^+ ions. Coordination of an F^- ion pulls these cations towards the centre of the cage. Swapping the central anion for Cl^-, Br^- and then I^- allows these cations to relax outwards. For the bare hosts $[\{HE(PH)_3Li_4{\cdot}3FH\}_4]$, the inner-shell Li^+ ions move further out, becoming "bumps" on the central cage rather than "dimples" (Figure 10).

Table 4. Selected bond lengths [Å] and angles [°] for the geometry-optimised structures examined.

X^-/E	B	Al	Ga	In
nothing				
E–P	2.093	2.439	2.465	2.614
P-E-P	112.7	107.6	107.0	104.2
P···P (bite)	3.489	3.938	3.961	4.125
centroid···Li(inner)	3.215	3.569	3.547	3.677
centroid···Li(outer)	3.982	4.041	4.042	4.055
centroid···E	3.712	4.077	4.115	4.287
F				
E–P	2.070	2.403	2.454	2.596
P-E-P	108.8	102.1	102.0	97.7
P···P (bite)	3.369	3.737	3.814	3.912
F···Li(inner)	1.974	2.024	2.077	2.067
F···Li(outer)	3.939	3.951	4.045	4.039
F···E	3.879	4.213	4.251	4.470
Cl[a]				
E–P	2.087	2.427	2.453	2.60
		[2.461(3)]	[2.432(1)]	[2.601(4)]
P-E-P	111.9	104.7	103.8	100.4
		[103.0(1)]	[102.82(4)]	[100.81(9)]
P···P (bite)	3.439	3.842	3.860	3.995
		[3.852(3)]	[3.802(2)]	[4.008(5)]
Cl···Li(inner)	2.458	2.535	2.524	2.565
		[2.45(1)]	[2.37(1)]	[2.46(3)]
Cl···Li(outer)	3.973	4.028	4.026	4.035
		[4.147(4)]	[3.887(1)]	[4.149(1)]
Cl···E	3.840	4.219	4.255	4.432
		[4.246(4)]	[4.256(1)]	[4.407(1)]
Br				
E–P	2.089	2.429	2.456	2.603
P-E-P	111.3	105.5	104.8	101.3
P···P (bite)	3.450	3.868	3.892	4.027
Br···Li(inner)	2.625	2.712	2.712	2.723
Br···Li(outer)	3.966	4.028	4.033	3.989
Br···E	3.837	4.204	4.241	4.409
I				
E–P	2.097	2.440	2.467	2.609
P-E-P	111.9	107.0	105.9	103.9
P···P (bite)	3.474	3.922	3.937	4.110
I···Li(inner)	2.819	2.976	2.959	3.009
I···Li(outer)	3.964	4.032	4.027	4.021
I···E	3.831	4.163	4.219	4.330

[a] Numbers in square brackets are the experimental values determined from the structures of **1**, **2** and **3**.

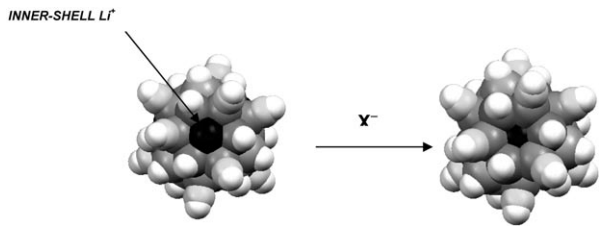

Figure 10. Coordination of halide ions (X^-) by the bare cages, showing the displacement of the inner-shell Li^+ ions towards the centre of the cage.

The energies of the coordination of halide ions (ΔE_R) by the bare hosts [{HE(PH)$_3$Li$_4$·3FH}$_4$] are given in Table 5.

Table 5. Energies geometry optimised structures [kJ mol^{-1}], constrained to *T*-symmetry, at the B3LYP/LACVP** level, relative to the energy of bare hosts and the isolated halide ions.

X$^-$/E	B	Al	Ga	In
nothing	0.00	0.00	0.00	0.00
F$^-$	−504.69	−404.66	−380.43	−469.69
Cl$^-$	−133.34	−121.10	−112.18	−142.94
Br$^-$	−84.17	−81.17	−72.25	−84.34
I$^-$	9.25	−25.92	−13.80	31.12

Examination of each row of Table 5 shows that F$^-$ is held most strongly by the B cage, Cl$^-$ by the In cage, and I$^-$ by the Al cage. Br$^-$ appears to show little selectivity, except that the Ga cage binds it less strongly than the others. A similar comparison cannot be made going down the columns of the Table 5, as the differences in energy are dominated by the charge density of the isolated halide ions. However, the data allows pairs of halide ions and pairs of bare hosts to be chosen, and the energetically favourable pairing to be determined. For example, Cl$^-$ and Br$^-$ ions will choose between Ga and In cages so that the Cl$^-$ ion is in the In cage and the Br$^-$ ion is in the Ga cage, since the total energy for this [−142.94 + (−72.25) = −215.19 kJ mol^{-1}] is lower than that for the corresponding pair with the halide ions interchanged [−112.18 + (−84.34) = −196.52 kJ mol^{-1}], even though bromide prefers the indium cage to the gallium one. The calculations therefore provide the first indication of selectivity in these systems and a template for further studies of anion coordination by these species.

Conclusion

The current study has shown that the Group 13 tetraanions [MeE(PPh)$_3$]$^{4-}$ (E = Al, Ga, In) can all be prepared, opening the way for more extensive coordination studies of these species with a range of main group and transition metals. Solid-state studies show that the complexes with LiCl form remarkably similar arrangements, in which the [{MeE(PPh)$_3$Li$_4$}$_4$(μ_4-Cl)]$^-$ ions adopt a highly unusual pseudo-primitive cubic (rather than close-packed) lattice. This suggests that the structure of all of the compounds is dictated by the desire to minimise anion–anion interactions, rather than to maximise cation–anion interactions. The location of the Li$^+$ counterions in these systems varies depending on the Group 13 element (E) present, and probably reflects small differences in factors such as lattice energy. The structure of the Al complex (**1**), containing a "naked" Li$^+$ ion) is of particular note since it provides a direct illustration of the concept of inverse coordination (i.e., of the anion of LiCl). Solid-state NMR studies have proved particularly useful in the characterisation of all of the compounds. These studies indicate the presence of a highly mobile/naked Li$^+$ ion in **1** which is replaced by THF-solvated Li$^+$ ions in **2** and **3**. These conclusions are broadly consistent with the results from low-temperature X-ray crystallographic studies, although the solid-state NMR studies are unable to detect the potential presence of a small fraction of uncoordinated Li$^+$ ions within the lattice of **2** (tentatively suggested by X-ray studies). DFT calculations have provided a framework for future structural investigations in this area, suggesting that a range of halide ions might be incorporated into these species and giving the first indication of potential anion-selective behaviour. Providing some validation for these theoretical investigations, we have recently been able to obtain the analogous bromide complexes which X-ray studies show to have the same type of cage [{MeE(PPh)$_3$Li$_4$·3THF}$_4$(μ_4-Br)]$^-$ ions as that found for **1**–**3**. A future paper will explore competitive coordination of halide anions.

Experimental Section

General: Compounds **1**, **2** and **3** are highly air- and moisture-sensitive. They were handled on a vacuum line (in an efficient cupboard) by using standard inert-atmosphere techniques and under dry/oxygen-free argon. *n*BuLi in hexanes and phenylphosphine were obtained from Aldrich. THF and diethyl ether were dried by distillation over sodium/benzophenone prior to the reactions. The products were isolated and characterised with the aid of a nitrogen-filled glove box fitted with a Belle Technology O_2 and H_2O internal recirculation system. Elemental analyses were performed by first sealing the samples under nitrogen in air-tight aluminium boats (1–2 mg) and C, H and N content was analysed using an Exeter Analytical CE-440 Elemental Analyser. P analysis was obtained by spectrophotometric means. ^{1}H, ^{7}Li and ^{31}P NMR spectra were recorded on a Bruker DPX 500 MHz spectrometer. ^{1}H NMR spectra were run in [D$_6$]benzene, using the solvent resonances as the internal standard. For ^{31}P NMR (referenced to an external standard of 85% H_3PO_4/D_2O) and ^{7}Li NMR (referenced to a saturated solution of LiCl/D_2O) non-deuterated THF was used as the solvent, using a [D$_6$]acetone capillary to obtain a lock.

Synthesis of 2 and 3: *n*BuLi (7.5 mL, 1.60 mol L^{-1} in hexanes, 12.0 mmol) was added to a stirred solution of $PhPH_2$ (0.66 mL, 6.00 mmol) in THF (50.0 mL) at room temperature. The yellow-green suspension produced was brought to reflux (4 h). A solution of $MeECl_2$ was added at room temperature (E = Ga (**2**), In (**3**)); prepared by addition of MeLi (1.25 mL, 1.6 mol L^{-1} in Et_2O) to a solution of ECl_3 (**2**: 0.35 g (2.0 mmol), **3**: 0.44 g (2.0 mmol)) in THF (20.0 mL) at −78 °C, followed by stirring at room temperature (45 min). The mixture was brought to reflux (14 h), to give dark brown solutions. After replacing the solvent by Et_2O (30.0 mL), heating to reflux for 5 min, and filtration (Celite, *P*3) to remove LiCl, the solvent was removed under vacuum and yellow-green precipitates were obtained. Crystallisation from THF (5.0 mL) at room temperature (48 h) led to yellow cube-shaped crystals of **2** or **3**. Compound **2**: Yield 0.23 g (16%, 2.0 mmol scale with respect to Ga). ^{1}H NMR (500.20 MHz, [D$_6$]benzene, 25 °C): δ = 8.3–6.9 (m, C-H Ph), 3.49 (m, -CH$_2$-O THF), 1.34 (m, -CH$_2$- THF), 0.40 ppm (s, Me-Ga); ^{31}P NMR (202.48 MHz, THF with [D$_6$]acetone capillary, 25 °C): δ = −150.5 (s, $W^1/_2$ = 350 Hz) (cf. **1** δ = −161.8 ppm); ^{7}Li NMR (194.40 MHz, THF with [D$_6$]acetone capillary, 25 °C), δ = 2.16 (br s), 1.75 (s), −0.55 ppm (s); elemental analysis calcd for **2** (%): C 56.9; H 6.7, P 12.9; found: C 54.3, H 6.6, P 12.0. Compound **3**: Yield 0.083 g (5.5%). ^{1}H NMR (500.20 MHz, [D$_5$]pyridine, 25 °C): δ = 7.7–6.9 (m, C-H Ph), 3.62 (m, -CH$_2$-O THF), 1.59 (m, -CH$_2$- THF), 0.03 ppm (s, Me-In); ^{31}P NMR (202.48 MHz, THF with [D$_6$]acetone capillary, +25 °C): δ = −166.1 ppm; ^{7}Li NMR (194.40 MHz, THF with [D$_6$]acetone capillary; +25 °C): δ = 1.44 (s),

−1.01 ppm (s; br shoulder at ca. $\delta = -0.6$ ppm); elemental analysis calcd (%) for **3**: C 53.5, H 6.3; P 12.2; C 52.5, H 6.0, P 11.6.

Crystal structures of 1, 2 and 3:[23] Crystals of **1**, **2** and **3** were mounted directly from solution under argon using an inert oil which protects them from atmospheric oxygen and moisture. X-ray intensity data were collected by using a Nonius Kappa CCD diffractometer. Details of the data collections and structural refinements are given in Table 1. The crystals of all three compounds are virtually isomorphous, crystallising in the cubic space group $F\bar{4}3c$. For all three crystals the positions of the non-hydrogen atoms of the anionic cluster were located by direct methods. Each cluster anion has the central chloride anion located on an eight-fold site of 23 symmetry (at $^1/_2$, $^1/_2$, $^1/_2$), surrounded tetrahedrally by four symmetry-related Li^+ ions and four $[MeE(PPh)_3]^{4-}$ units (each with C_3 symmetry) with the P atoms bridged by an additional twelve symmetry-related Li-$(THF)^+$ groups. Effectively the "spherical" 326 atoms cluster anions are located on all the lattice points of the *F*-centred cubic unit cell *and* all the interstitial octahedral sites, that is, the crystals could be regarded as a NaCl-type structure with the Na^+ and Cl^- sites all occupied by the giant anions. For **2** and **3**, residual electron density in subsequent Fourier-difference maps was interpreted as due to THF molecules of solvation and these were included in the refinement with site occupancy of $^1/_4$ giving a total of three lattice THF molecules per cluster anion. The site of the eight lithium cations per unit cell, required for electroneutrality, is problematic owing to the very high symmetry of the cubic space group of these structures. The only eight-fold site remaining at ($^1/_4$, $^1/_4$, $^1/_4$) was ruled out for Li^+ as it is at the centre of a void of with a radius of about 8 Å. The most reasonable location for a naked Li^+ ion is midway between cluster anions along the edge of the cubic unit cell and at $^1/_4$, 0, 0 (site symmetry −4)], that is, $^1/_3$ Li^+ occupancy in each of these twenty-four symmetry related sites (balancing the −8 charge of the eight anions present) (Figure 3). In the lattice of **1**, which showed no evidence of lattice solvent molecules, residual electron density of about 1 eÅ^{-3} was found at this position (but not in **2** and **3**), and a Li atom of $^1/_3$ occupancy was assigned to this site. In support of this location is the observation that it allows the Li^+ ions to loosely bind two cluster anions together through agostic C–H···Li interactions with four symmetry-related THF ligands (C···Li ca. 2.85–3.17 Å). The presence of THF solvent molecules in the lattice of **2** and **3** raises the possibility that these donor molecules might provide an alternative site for the Li^+ counterion. In both compounds the solvate THF molecules are about 2 Å from a crystallographic C_3 axis and it seems probable that they are held in this close proximity to each other by coordination to an undetected Li^+ ion located on the C_3 axis (residual electron density for a $^1/_4$ occupancy Li is unlikely to be observed). For **3**, a Li^+ atom of this occupancy was included on the C_3 axis at the centroid of the three THF donor oxygen atoms and the resulting $Li(THF)_3^+$ units refined satisfactorily. The situation in the Ga compound **2** is complicated by a disorder of the $^1/_4$ occupancy THF solvates in which one third of the potential donor oxygen atoms are not within bonding distance of the C_3 axis and attempts to refine a Li atom of $^1/_4$ occupancy on the C_3 axis gave impossibly high ADP. The most satisfactory solution appears to be an allocation of $^2/_{12}$ Li^+ ions to the C_3 site (i.e., equivalent to the major component of the disordered THF) and the remaining $^1/_{12}$ Li^+ to the site at ($^1/_4$, $^1/_4$, $^1/_4$), observed in the structure of **1**. This combination gave satisfactory refinement. In **2** and **3**, residual electron density of about 2–4 eÅ^{-3} was found at the periphery of the cluster anions in a site centrosymmetrically related through the central Cl^- ion to the position of the Ga or In atoms. This was interpreted for each as disorder of a small amount of a similar cluster anion of the opposite hand, randomly distributed at the same site throughout the crystal; no electron density due to the lighter atoms of the minor component could be detected. The final difference-Fourier for the Al cluster **1** (communicated previously) was re-examined and a similar site of residual density (ca. 1 eÅ^{-3}) to that detected in **2** and **3** was observed. The minor component of the metal atom for each of the anions **1**, **2** and **3** was included in the refinement which was based on F^2 and **2** was refined as a twin. The hydrogen atoms for all three structures were placed in calculated positions with displacement parameters set equal to 1.2 U_{eq} (or 1.5 U_{eq} for methyl groups) of the parent carbon atoms. In the final cycles of full-matrix least-squares refinement, the non-hydrogen full-occupancy atoms were assigned anisotropic displacement parameters.

CCDC-267276 (**1**), CCDC-609522 (**2**) and CCDC-609523 (**3**) contain the supplementary crystallographic data for this paper. These data can be obtained free of charge from The Cambridge Crystallographic Data Centre via www.ccdc.cam.ac.uk/data_request/cif.

Solid-state NMR spectroscopy: Solid-state NMR experiments were performed on a Bruker Avance-AQS spectrometer tuned to 399.88 MHz for ^{1}H, 161.84 MHz for ^{31}P, 155.41 MHz for ^{7}Li, and 58.85 MHz for ^{6}Li. A Bruker 4-mm double-resonance probe was used for all experiments, with spinning stabilised to ±3 Hz using standard Bruker equipment. The aluminium complex (**1**) was spun at 12 kHz for all experiments, while the gallium and indium analogues (**2** and **3**, respectively) were spun at 6 kHz unless otherwise noted. Dry nitrogen was used to spin the samples, minimising contact with oxygen present in the air. TPPM[25] or SPINAL-64[26] ^{1}H-decoupling at approximately 100 kHz was performed for all experiments unless otherwise noted. ^{7}Li spectra were referenced externally to 1.0 mol L^{-1} $LiCl_{(aq)}$ at 0 ppm. ^{1}H to ^{7}Li cross-polarisation (CP) under magic angle spinning (MAS) used a 500 μs contact time and an 8 s recycle delay. 80 transients were collected. The spectral width was 12 kHz; acquisition was performed for 15 ms. Longitudinal relaxation time constants T_1 were determined by using a saturation-recovery experiment in which magnetisation was monitored as a function of delay τ following saturation. The experiment on **1** was performed with no decoupling (which had only a small effect on line shape and peak width). A total of 1000 17-μs effective 90° pulses separated by 20-ms delays were used for saturation of **1**; the same length pulse was used as a readout pulse following τ. A total of 60 τ values logarithmically distributed between 0.01 s and 159.5 s were used in the experiment, and 20 transients were acquired of each τ slice. The recycle delay was 5 s. The spectral width was 12 kHz; 186 complex points were acquired. The spectrum was zero-filled to 512 points before Fourier transformation. Following Fourier transformation, an inverse Laplace transformation was performed for each f_2 point. 80 time values distributed logarithmically between 0.1 s and 240 s were used in the search for the inverse Laplace transform. For the Ga (**2**) and In (**3**) analogues, ^{1}H-decoupling was performed during acquisition. A total of 80 τ values logarithmically distributed between 0.01 s and 300 s were used; 20 transients were co-added for each slice. The recycle delay was 5 s. The spectral width was 6 kHz and 229 complex points were acquired for each FID. For **2**, 200 16.5-μs effective 90° pulses separated by 2-ms were used for saturation, while for **3**, 300 16-μs effective 90° pulses separated by 20 ms were used for saturation. In each case, the same effective 90° pulse was used to read out magnetisation before acquisition. For **2**, 40 Hz of exponential line broadening was applied and the spectrum was zero-filled to 1024 points before Fourier transforming in t_2. For **3**, 40 Hz of exponential line broadening was applied and the spectrum was zero-filled to 768 points. In both cases, 160 time values distributed logarithmically between 0.01 s and 300 s were used in the search for the inverse Laplace transform.

The ^{6}Li ^{1}H-decoupled spectrum acquired of **1** was referenced externally to 1.0 mol L^{-1} LiI(aq) at 0 ppm. Continuous-wave decoupling was applied at 80 kHz. A total of 930 transients were acquired with a spectral width of 20 kHz; acquisition was performed for 45 ms. ^{31}P NMR spectra were externally referenced to hydroxyapatite which has a chemical shift of 2.3 ppm relative to 85% H_3PO_4. Four scans were acquired of **1** using 100-kHz pulses on ^{31}P. The spectra width was 100 kHz and signal was acquired for 5.1 ms. A 60 s recycle delay was used. Thirty-two scans were acquired of **2**. The position of the isotropic peak was established by comparing spectra acquired at 5 and 6 kHz. Thirty-two scans were acquired using 100 kHz pulses on ^{31}P. The spectral width was 100 kHz; the acquisition time was 4.7 ms. A 20 s recycle delay was allowed. The same parameters were used for **3**, except that 96 scans were acquired.

^{13}C NMR spectra were referenced externally using the carbonyl signal in glycine at 176.04 ppm. Ramped cross-polarisation[27] was used with a contact time of 1500 μs. A total of 256 scans were acquired in the CPMAS spectra of each compound; a 10 s recycle delay was used. The spectra width was 90 kHz and the acquisition time 30 ms. The same conditions were used for acquiring CP-TOSS spectra[28] of **1**–**3**, with the addition of

83 kHz ^{13}C 180° pulses. A total of 256 scans were acquired for **2** and 400 for **3**.

Acknowledgements

We thank Dr. John Davies (Cambridge University) for collection of the X-ray data. We gratefully acknowledge the EPSRC (M.J.D., F.G., J.M.G., M.McP. and M.L.S.) and Gates Trust (Cambridge) and The National Science Foundation (R.S.) and The EU (Erasmus grant for J.P.H.) and The Konrad-Adenauer-Stiftung (J.P.H.) for financial support. Acknowledgement is made to the donors of the American Chemical Society Petroleum Research Fund for partial support of this research (M.L.S).

[1] R. Snaith, D. Wright in *Lithium Chemistry; A Theoretical and Experimental Overview* (Eds.: A.-M. Sapse, P. von R. Schleyer), Wiley, **1994**, Chapter 8, pp. 227.

[2] For example see: A. Lupulescu, M. Kotecha, L. Frydman, *J. Am. Chem. Soc.* **2003**, *125*, 3376; S. M. Ivanova, B. G. Nolan, Y. Kobayashi, S. M. Miller, O. P. Anderson, S. H. Strauss, *Chem. Eur. J.* **2001**, *7*, 503.

[3] D. Barr, W. Clegg, R. E. Mulvey, R. Snaith, *J. Chem. Soc. Chem. Commun.* **1984**, 79.

[4] J. Sloan, A. I. Kirkland, J. L. Hutchison, M. L. H. Green, *Chem. Commun.* **2002**, 1319.

[5] Mulvey and co-workers have coined the term *inverse crowns* to describe a series of macrocycles composed of Group 1 and/or 2 metal acceptors linked by amido groups, R. E. Mulvey, *Chem. Commun.* **2001**, 1049; R. E. Mulvey, *Organometallics* **2006**, *25*, 1060.

[6] For examples of organic receptors of this type, see: J. L. Sessler, J. M. Davis, *Acc. Chem. Res.* **2001**, *34*, 984.

[7] So-called "metallacarboran" macrocycles composed of acceptor Hg^{II} ions linked by C_2B_{10} icosahedra: M. F. Hawthorne, Z. Zheng, *Acc. Chem. Res.* **1997**, *30*, 267.

[8] P. J. M. W. Birker, J. Reedijk, G. C. Verschoor, *Inorg. Chem.* **1981**, *20*, 2877; R. Wang, T. Jin, Z. Zheng, R. J. Staples, *Angew. Chem.* **1999**, *111*, 1929; *Angew. Chem. Int. Ed.* **1999**, *38*, 1813; A. Müller, R. Rohlfing, R. Krichemeyer, E. Penk, H. Bögge, *Angew. Chem.* **1993**, *105*, 916; *Angew. Chem. Int. Ed. Engl.* **1993**, *32*, 909; Z. Zheng, *Chem. Commun.* **2001**, 2521.

[9] A. D. Hopkins, J. A. Wood, D. S. Wright, *Coord. Chem. Rev.* **2001**, 155, 216; M. A. Beswick, N. Choi, C. N. Harmer, A. D. Hopkins, M. McPartlin, D. S. Wright, *Science* **1998**, *281*, 1500; F. García, A. D. Hopkins, C. M. Pask, D. S. Wright, *J. Mater. Sci.* **2004**, *39*, 3093.

[10] Isoelectronic nitrogen analogues $[RAl(NAr)_3]^{4-}$ (R = Et, *n*Bu; Ar = 2-$MeOC_6H_4$) have recently been reported: M. C. Copsey, J. C. Jeffery, C. A. Russell, J. M. Slattery, J. A. Slaughan, *Chem. Commun.* **2003**, 2306.

[11] M. J. Duer, F. Garcia, R. A. Kowenicki, V. Naseri, M. McPartlin, M. L. Stead, R. Stein, D. S. Wright, *Angew. Chem.* **2005**, *117*, 5875; *Angew. Chem. Int. Ed.* **2005**, *44*, 5729.

[12] The dilithiation procedure is the same as that reported previously for a range of other primary phosphines, see: K. Niediek, B. Neumüller, *Z. Anorg. Allg. Chem.* **1993**, 885, 619. Whether the reaction of $PhPH_2$ with *n*BuLi produces a *genuine* dilithiate could not be ascertained by NMR spectroscopy due to the low solubility of the product. Attempts to prepare **1** by stepwise reaction of $MeAlCl_2$ with $PhPH_2$ followed by reaction with *n*BuLi failed. The presence of 2 equivalents of *n*BuLi in the reaction mixture prior to reaction with $MeAlCl_2$ is necessary to prevent an alternative pathway involving P–P bond formation, see: F. García, S. M. Humphrey, R. A. Kowenicki, M. McPartlin, D. S. Wright, *Dalton Trans.* **2004**, 977.

[13] S. Berger, S. Braun, H.-O. Kalinowski, *NMR Spectroscopy of the Non-Metallic Elements*, Wiley, Chichester, **1996**, Ch. 7, p. 700; J. H. Letcher, J. R. van Wazer, *Top. Phosphorus Chem.* **1967**, 5, 75; J. H. Letcher, J. R. van Wazer, *J. Chem. Phys.* **1966**, *44*, 815.

[14] A similar structural trend has been observed previously in the antimony complexes $[Sb(ER)_3]^{3-}$ (E = N or P); see: M. A. Beswick, N. Choi, C. N. Harmer, A. D. Hopkins, M. A. Paver, M. McPartlin, D. S. Wright, *Inorg. Chem.* **1998**, *37*, 2177; M. A. Beswick, C. N. Harmer, R. R. Raithby, D. S. Wright, *Chem. Commun.* **1997**, 1897.

[15] The C···Li distances involved are typical of agostic interactions in a range of organolithium compounds, see: W. Setzer, P. von R. Schleyer, *Adv. Organomet. Chem.* **1985**, *24*, 353; W. Scherer, P. Sirsch, D. Shorokhov, G. S. McGrady, S. A. Mason, M. G. Gardiner, *Chem. Eur. J.* **2002**, *8*, 2324.

[16] J. M. Thomas, L. A. Bursill, E. A. Lodge, A. K. Cheetham, C. A. Fyfe, *J. Chem. Soc. Chem. Commun.* **1981**, 276.

[17] J. L. Markley, W. J. Horsley, M. P. Klein, *J. Chem. Phys.* **1971**, *54*, 3604.

[18] A. Lupulescu, M. Kotecha, L. Frydman, *J. Am. Chem. Soc.* **2003**, *125*, 3376.

[19] T. Roths, M. Marth, J. Weese, J. Honerkamp, *Comput. Phys. Commun.* **2001**, 279, 139.

[20] The ideal saturation-recovery curves were made to approximate actual saturation-recovery curves by the addition of 0.5% noise (noise having a standard deviation equal to 0.5% intensity of the most intense point in the curve), and the inverse Laplace transform of the noisy curves were then taken. The inverse Laplace transform examined 120 time values logarithmically distributed between 0.01 s and 300 s. This process was repeated 100 times to investigate the reliability of the inverse Laplace transform. For the inverse Laplace transform for the curves with $T_1 = 10$ s, all fits found the correct maximum but the standard deviation curve indicates that the greatest variation among the 100 fits performed occurs in the linewidth of the peak fit. Noise, therefore, often appears in the inverse Laplace transform as a broadened peak. It may also appear as a low-intensity component with T_1 at either the high or the low end of the range searched over in the inverse Laplace transform. Such a low-intensity component appeared in approximately 10% of the fits obtained. In each case, the low-intensity component had less than 2% of the intensity of the large peak in the fit. For the average inverse Laplace transform for the curves with one component having $T_1 = 10$ s present with seven times greater intensity than a second component with $T_1 = 100$ s, every inverse Laplace transform found two components in the simulated saturation-recovery spectrum, but the second T_1 value was consistently overestimated. This did not occur when simulated curves with only component with $T_1 = 100$ s were transformed.

[21] A. D. Becke, *J. Chem. Phys.* **1993**, *98*, 5648; C. Lee, W. Yang, R. Parr, *Phys. Rev. B* **1988**, 785, 37.

[22] P. J. Hay, W. R. Wadt, *J. Chem. Phys.* **1985**, *82*, 299.

[23] Jaguar 4.2, Schrödinger, Inc.: Portland, Oregon, **2000**.

[24] G. M. Sheldrick, G. M. SHELX-97, Göttingen, **1997**.

[25] A. E. Bennett, C. M. Rienstra, M. Auger, K. V. Lakshmi, R. G. Griffin, *J. Chem. Phys.* **1995**, *102*, 6951.

[26] B. M. Fung, A. K. Khitrin, K. Ermolaev, *J. Magn. Reson.* **2000**, 97, 142.

[27] G. Metz, X. Wu, S. Smith, *J. Magn. Reson. Ser. A* **1994**, 219, 110.

[28] W. T. Dixon, J. Schaefer, M. D. Sefcik, E. O. Stejskal, R. A. McKay, *J. Magn. Reson.* **1982**, 341, 49.

Received: June 5, 2006
Published online: November 6, 2006

